Drop Encapsulated in Bubble: A New Encapsulation Structure

Yingnan Shen, Liang Hu,[*] Wenyu Chen, Haibo Xie, and Xin Fu

The State Key Laboratory of Fluid Power and Mechatronic Systems, Zhejiang University,
38 Zheda Road, Hangzhou 310027, China

A new fluid encapsulation structure, which is characterized by a bubble encapsulating a drop, is reported. It is stably generated from the breakup of a liquid column inside a bubble, which is achieved via the injection of Taylor flow into liquid. A model is constructed to explain the liquid column breakup mechanism. A dimensionless control guidance, which enables the possibility to create different-scale capsules, is provided. The encapsulation stability in external flows is verified, and a method to trigger the release of the encapsulated drop is provided, which supports potential applications with great advantages such as fluid transport.

Fluid encapsulation, which is the physical phenomenon of one fluid encapsulating another fluid, can be classified into three major branches: "air in liquid," "liquid in liquid," and "liquid in air," as shown in Fig. 1(a). The air in liquid structure is most well known as soap bubbles with liquid films that encapsulate gas pockets. This structure also forms when a bubble is encapsulated in a drop [1–3]. The liquid in liquid structure is commonly called an emulsion, which is produced by a drop of one liquid encapsulating a smaller drop of a second liquid [4,5]. Another case is called drop coating, where the drop is coated with a liquid film with a thickness of only approximately $1/10^3$ of the drop diameter [6]. The liquid in air structure is commonly known as antibubbles, where the drop is encapsulated by an air film with a thickness of only approximately $1/10^4$ of the drop diameter [7,8]. Thus, the known encapsulation structures can also be classified into two groups based on the ratio of the shell thickness h to the overall diameter D: thin shell $(h/D < 1/10^3)$ and thick shell $(h/D > 1/10)$. Currently, the encapsulation of drops by thick air shells is the last unknown area in the fluid encapsulation map.

The interesting phenomenon called "drop encapsulated in bubble" was discovered when we developed immersion lithography machines. The air phase here, which encapsulates the drop, is no longer a thin film but a bubble. It is the exact structure of a drop encapsulated by a thick air shell, which is an important supplement for fluid encapsulation phenomena. As shown in Fig. 1(b), this encapsulation structure is generated by the injection of Taylor flow into bulk liquid: first, a gas slug forms a bubble; then, the following liquid slug penetrates the bubble and evolves into a liquid column; finally, the liquid column breaks up into a drop which is encapsulated in the bubble. The Taylor flow is formed by the development of the air-liquid mixture in a vertical microchannel (inner diameter $d = 1.0/0.5/0.3$ mm), which is analogous to the flow field in immersion hoods studied in our previous work [10,11]. The gas and liquid flow rates were adjusted within 10–80 and 3–20 mL/ min. Experiments were performed on aqueous glycerol solutions that contained 0–70% (mass fraction, w_g) glycerol. As shown in Fig. 1(c), the capsules were continuously produced with consistent features in a long period of 3886 ms.

The mechanism of a bubble encapsulating a drop is related to an intriguing question: how does a drop formation process complete inside a bubble? First, as shown in Fig. 2(a), a liquid slug reaches the nozzle to induce the bubble detachment and subsequently penetrates the bubble. A liquid column erects in the bubble, whose morphology is similar to the liquid column formed when a drop partially coalesces at a liquid interface [12]. The classic mechanism of drop formation from a liquid column is through Rayleigh-Plateau instability [13]. However, for short liquid columns that occur in partial coalescence, the wavelike instability cannot be observed, and simulations were performed to prove that breakup would not occur without an initial upward motion [14]. The simulations can be verified by our experiments: as shown in Fig. 2(b), the liquid column that erects on the liquid surface stops rising upward at time 0 and coalesces into the liquid surface before the breakup. Additionally, in the breakup situations as shown in Figs. 2(c)–2(f), the wavelike instability never occurs along the liquid columns. Thus, the notion that Rayleigh-Plateau instability causes the breakup can be denied.

The liquid column breakup is determined by the competition between two surface-tension-driven processes, radial necking and axial contraction, which also occur in partial drop coalescence [14] and free liquid column breakup [15]. However, in partial coalescence, the radial necking critically depends on the early dynamics when a drop gradually evolves into a column. Compared with free-liquid columns, the liquid columns in Fig. 2 should be classified as "single-ended" columns, which connect with a liquid surface and have only one free end. The dynamics of a liquid column is controlled by the surface tension,
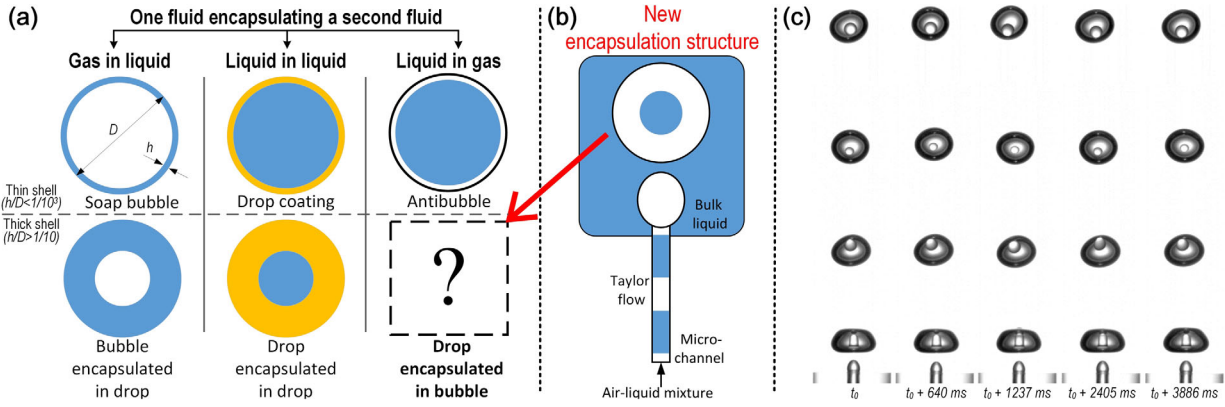
FIG. 1. (a) Drop encapsulated in bubble, which is the last unknown area in the fluid encapsulation map. (b) Diagram of the experiment setup. (c) Stable production of uniform capsules (see Supplemental Material for the multimedia view [9]).

viscosity, and inertia. The ratio of surface tension to viscosity is expressed by the Ohnesorge number $Oh = \mu/\sqrt{\rho\sigma R}$, where μ, ρ, and σ are the viscosity, density, and surface tension of the liquid, respectively, and R is the liquid column radius. When the liquid column is sufficiently long, the breakup is only determined by Oh [16]. For short columns, the aspect ratio L_0 also plays an important role in determining the breakup. The liquid column in Fig. 2(b) is notably low in Oh but still fails to break up without a sufficiently large L_0. The encapsulation demands an effectively stretched single-ended liquid column with a sufficiently large L_0 at its Oh to break up inside a bubble. As shown in Figs. 2(c) and 2(d), the liquid column evolves into a liquid bridge across the bubble and stretches as the bubble rebounds. The liquid bridge pins continually shrink until the smaller pin breaks up, and an effectively stretched single-ended liquid column is produced. In some situations, as seen in Fig. 2(e), the liquid column can be stretched to a sufficiently large L_0 by liquid convergence to its top. In high-Oh conditions in Fig. 2(f), the liquid column demands a much larger L_0 to break up.

When a single-ended liquid column is formed, the radial necking and axial contraction processes begin to compete.

The total time of the radial necking process can be scaled with a characteristic time. Here, we define a critical Ohnesorge number Oh_C. When $Oh > Oh_C$, the viscosity and surface tension dominate, which gives the characteristic time $t_v = \mu R/\sigma$. When $Oh < Oh_C$, the inertia and surface tension dominate, which gives the characteristic time $t_i = R\sqrt{\rho R/\sigma}$. Thus, the total time is $t_n = \alpha t_v$ when $Oh > Oh_C$ and $t_n = \beta t_i$ when $Oh < Oh_C$, where α and β are prefactors. Encapsulation events are plotted in terms of R and t_n in Fig. 3. The expression neglecting viscosity ($Oh < Oh_C$) is plotted with a solid line consistent with the experiment data when $\beta = 3.2$. The expression neglecting inertia ($Oh > Oh_C$) is plotted with dotted lines and consistent with the experiment data at all viscosities when $\alpha = 62$. The prefactors α and β indicate the time distances from the singularity where the viscous and surface tension forces are balanced, and the singularity where the inertial and surface tension forces are balanced. Compared with the existing breakup models, when we use the slender-jet equations [17], we can predict that $\alpha \approx 33$, which is smaller than the situation of single-ended columns in our study; using the full inviscid equations [18], we can predict that $\beta \approx 3$, which corresponds to the value obtained in our study.
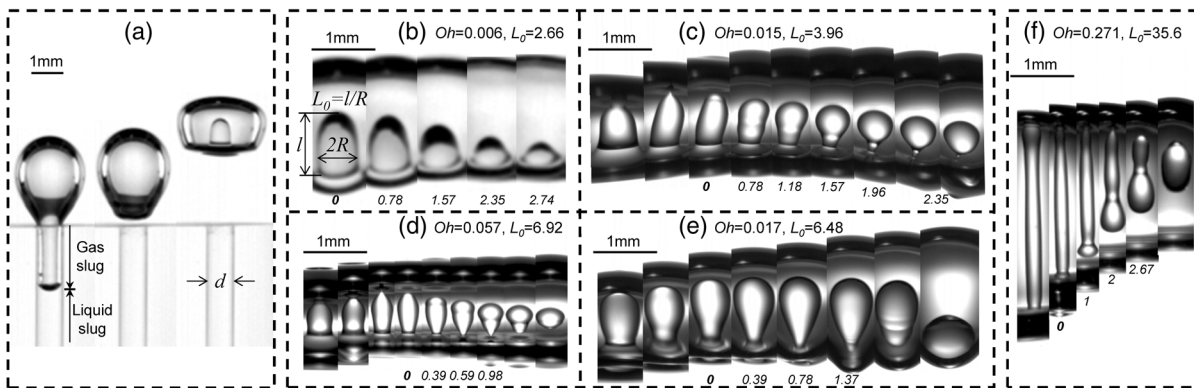

FIG. 2. (a) Injection of Taylor flow into the liquid makes a liquid column penetrate a bubble; (b) the liquid column fails to break up with a small aspect ratio L_0; (c)–(f) at various Oh, the encapsulation structure is generated by the breakup process of a liquid column with a sufficiently large L_0.
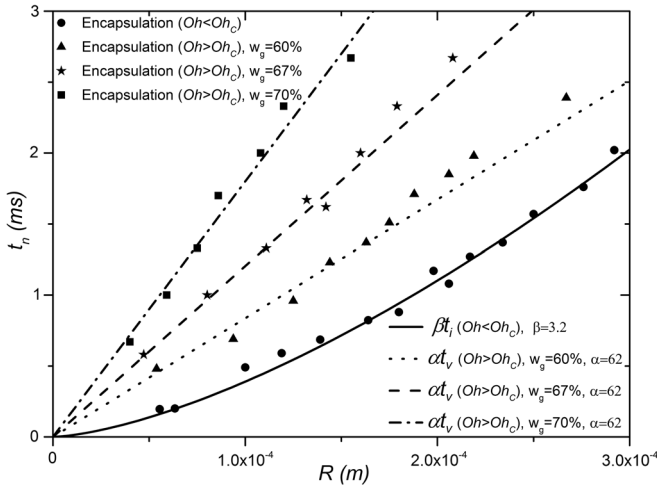
FIG. 3. Encapsulation events plotted in terms of the liquid column radius R and radical necking time t_n (circle: $Oh < Oh_C$; triangle: $Oh > Oh_C$ and $w_g = 60\%$; star: $Oh > Oh_C$ and $w_g = 67\%$; square: $Oh > Oh_C$ and $w_g = 70\%$). The solid line indicates the model $t_n = \beta t_i$ when $Oh < Oh_C$, and the other three lines indicate the model $t_n = \alpha t_v$ when $Oh > Oh_C$.

FIG. 4. Phase diagram showing the outcome of the experiments (solid circle: encapsulation; open circle: no encapsulation) in terms of Oh—L_0. The thick solid line indicates our model of the critical aspect ratio: $L_{0C} = \beta$ for $Oh < 0.052$ and $L_{0C} = \alpha Oh$ for $Oh > 0.052$. The light black line is the model in Ref. [22]. The light dashed line indicates the limit L_{0M} on the increase in aspect ratio. The thick dashed line indicates the location of Oh_C.

By assuming $\alpha t_v = \beta t_i$, the critical Ohnesorge number is obtained: $Oh_C = \beta/\alpha = 0.052$.

For an asymmetric free liquid column, the axial length scale is significantly larger than the radial length scale, particularly near the breakup [19]. The axial contraction velocity does not depend on the viscosity outside the viscous length scale $L_v = \mu^2/\rho\sigma$ [20], which is below 4.7 μm in this study, so it only relates to the Taylor speed $V_T = \sqrt{2\sigma/\rho R}$ [21]. When the capillary pressure is included, the axial contraction velocity is given by $V_a = V_T/\sqrt{2} = \sqrt{\sigma/\rho R}$ [20]. Both free ends move to the midpoint at identical speed, so the liquid column is commonly computed in terms of only one end. The single-ended liquid column in drop-on-demand inkjet printing, which consists of a spherical head followed by a column, is considered equivalent to a double-length free-liquid column [22]. In our opinion, this equivalence is only reasonable when the head is significantly more massive than the column, which guarantees that the mass point locates under the column. In our study, the column connects with the bulk liquid, so this equivalence is certainly applicable. Therefore, the total time of axial contraction is $t_c = l/V_a = l\sqrt{\rho R/\sigma}$, where l is the column length. The criterion for encapsulation is that the liquid column breaks up before the axial contraction ends, so the critical encapsulation conditions are determined by assuming $t_n = t_c$. The aspect ratio is $L_0 = L/2R = l/R$, where L is the length of the equivalent free liquid column, and $L = 2l$. At every Oh there exists a critical aspect ratio L_{0C}, beyond which the encapsulation should occur. When $Oh < Oh_C$, we assume $t_n = \beta t_i = t_c$, giving $L_{0C} = \beta$. When $Oh > Oh_C$, we assume $t_n = \alpha t_v = t_c$, giving
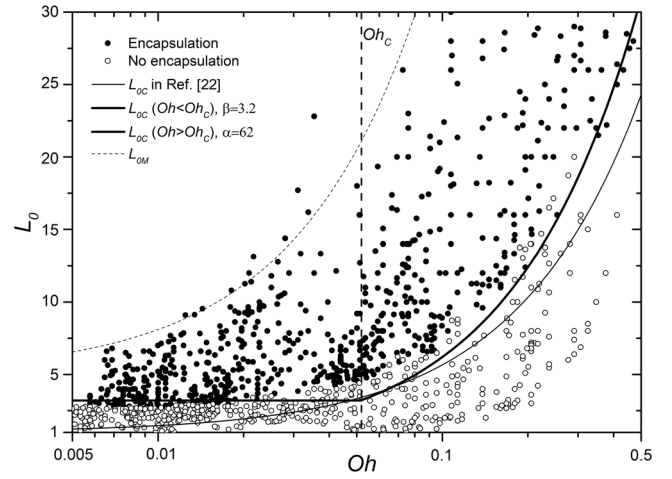
$L_{0C} = \alpha Oh$. The experiment results are plotted in terms of L_0 and Oh in Fig. 4. The prediction from the model is plotted as thick curves, and the model in Ref. [22] is also shown (thin line) in Fig. 4. For comparison, our model is more reasonable to neglect viscosity below Oh_C. When $Oh < Oh_C$, there is a lower limit for L_{0C}, which is irrelevant to Oh and consistent with the value predicted by the model: 3.2, which is identical to β. When $Oh > Oh_C$, the experimental L_{0C} is also reasonably consistent with the model and linearly increases with Oh at a rate of 62, which is identical to α.

Each single-ended liquid column with the required $L_0 > L_{0C}$ for breakup is generated by a liquid column impacting on a bubble. In addition, there is a limit L_{0M} on the increase in aspect ratio in Fig. 4, which is also attributed to the impact dynamics. The control parameters that affect the impact dynamics are the liquid column velocity v, liquid viscosity μ, column diameter (upon the impact) d, and bubble radius R_B (calculated from the gas slug volume). When μ varies, the critical encapsulation events are plotted in terms of $v - d/R_B$ in Fig. 5(a). In the impact process, the penetration of the liquid column into the bubble is driven by the inertia of the liquid column while resisted by the pressure in the bubble. The liquid column inertia is described by the Reynolds number $Re = \rho v d/\mu$, which is the ratio of inertia to viscosity effect. The difference between the bubble interior pressure P_B and the bulk liquid pressure P_L is $\Delta P = P_B - P_L = 2\sigma/R_B$. Hence, the resistance force is $\Delta P(\pi d^2/4) = \pi\sigma d^2/2R_B$. Scaled by the bubble surface tension force, the resistance effect is $(\pi\sigma d^2/2R_B)/(2\pi\sigma R_B) \sim d^2/R_B^2$. Thus, the impact dynamics (i.e., penetration of the liquid column) can be
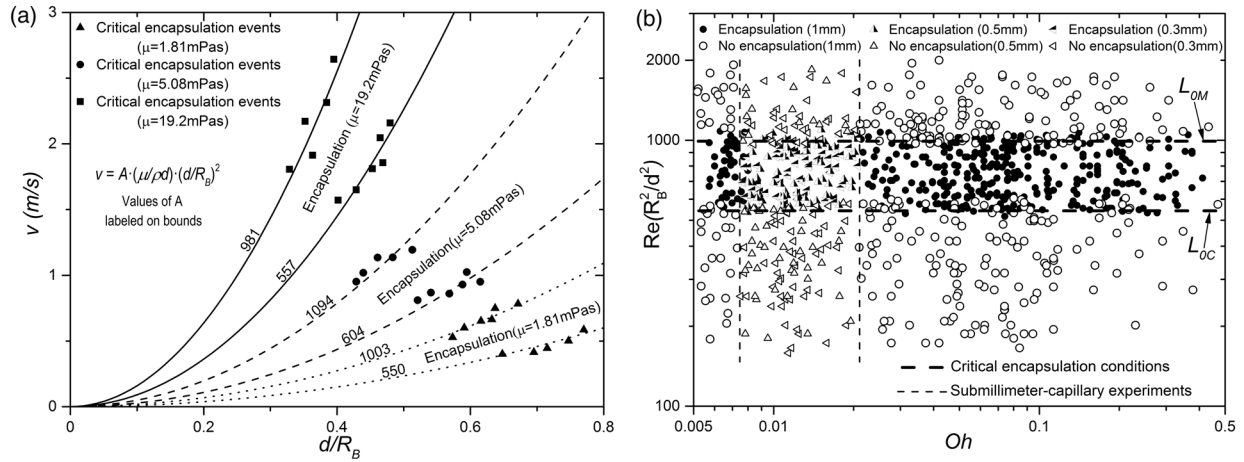
FIG. 5. (a) Critical encapsulation events plotted in terms of $v - d/R_B$ at different viscosities (triangle: $\mu = 1.81$ mPa s; circle: $\mu = 5.08$ mPa s; square: $\mu = 19.2$ mPa s). The solid, dashed, and dotted lines indicate the encapsulation region bounds with different μ. (b) Phase diagram of the control guidance in terms of $\mathrm{Re}(R_B^2/d^2)$ to produce single-ended liquid columns with $L_{0C} < L_0 < L_{0M}$ at any Oh.

characterized by the ratio of driving to resistance effect using $\mathrm{Re}/(d^2/R_B^2)$. The Weber number of the liquid column ($We = \rho d v^2/\sigma$) ranges from 1.86 to 106. In this studied range, the Weber number does not play a significant role in the outcome of the impact. In Fig. 5(a), the experiment results are consistent with the relation of $\mathrm{Re} \propto d^2/R_B^2$. With different viscosities, the experiment data at lower and upper bounds for encapsulation are fitted in terms of $v = A(\mu/\rho d)(d^2/R_B^2)$, where A is a prefactor. At the lower bounds where $A \approx 550$, the ratio of driving to resistance effect enables the liquid column to be stretched to $L_0 = L_{0C}$; when $A < 550$, the liquid column with $L_0 < L_{0C}$ coalesces into the bulk liquid below the bubble. At the upper bounds where $A \approx 1000$, the increase of L_0 ceases close to L_{0M}; when $A > 1000$, the entire liquid column passes through the bubble and coalesces into the bulk liquid above the bubble. Thus, as shown in Fig. 5(b), to produce this encapsulation structure, we can control the

Taylor flow to satisfy $550 < \mathrm{Re}(R_B^2/d^2) < 1000$, where the generated single-ended liquid column at every Oh can satisfy the breakup criterion of $L_{0C} < L_0 < L_{0M}$. The relation between R_B and d indicates the predictive capability to further scale down the capsule size.

For potential industrial applications, the ability of this encapsulation structure to maintain stability in external flows has been verified, and a method to trigger the release of the encapsulated drop is provided. Emulsions have been applied in industrial activities such as drug delivery [23] and material processing [24]. However, when delivered in a shear flow, the inner drop is stretched in tandem with the outer drop and eventually breaks up [25,26]. Antibubbles have aroused great interest for potential applications such as fluid transport [27]. However, the breakup of the air film is immediately triggered under external pressures as low as 2 kPa [28,29].

The encapsulation stability faced with a sudden shear flow is shown in Fig. 6(a). Although the bubble severely deforms,
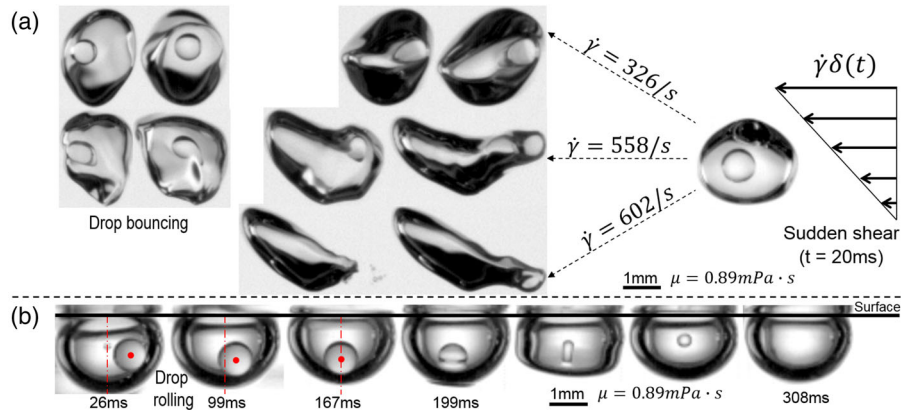

FIG. 6. (a) Encapsulation stability with a sudden shear flow. (b) Release of the encapsulated drop by depositing the capsule on a surface.

the drop continues being encapsulated until the shear rate $\dot{\gamma}$ increases to 602/s. The outer shell (bubble) does not break up like an antibubble, and the inner core (drop) does not deform with the outer shell like an emulsion. As shown in Fig. 6(b), when a capsule deposits on a liquid or solid surface ($t = 0$), the bubble stops deforming, and the encapsulated drop stops bouncing. The drop rolls on the bubble surface figuratively like a pendulum that swings increasingly slowly until it deposits at 167 ms. After a deposition period of 32 ms, the drop begins to coalesce into the surrounding liquid. The drop fully merges at 308 ms through a series of partial coalescence processes. Thus, the encapsulation stability relies on bubble deformations, which continuously produce relative displacements between the bubble and the drop and consequently prevents the drainage of the interstitial air layer. The capsule can be stably transported even in strong shear flows, and we can control the encapsulated drop to be quickly released by making the capsule deposit on a surface. Hence, we can expect its potential applications with great advantages such as fluid transport.

---

*Corresponding author.
cmeehuli@zju.edu.cn

[1] D. Bartolo, C. Josserand, and D. Bonn, Phys. Rev. Lett. **96,** 124501 (2006).

[2] O. Vincent, P. Marmottant, P. A. Quinto-Su, and C. D. Ohl, Phys. Rev. Lett. **108,** 184502 (2012).

[3] W. J. Duncanson, A. Abbaspourrad, H. C. Shum, S. H. Kim, L. L. Adams, and D. A. Weitz, Langmuir **28,** 6742 (2012).

[4] A. S. Utada, E. Lorenceau, D. R. Link, P. D. Kaplan, H. A. Stone, and D. A. Weitz, Science **308,** 537 (2005).

[5] S. S. Datta, S. H. Kim, J. Paulose, A. Abbaspourrad, D. R. Nelson, and D. A. Weitz, Phys. Rev. Lett. **109,** 134302 (2012).

[6] I. Polenz, D. A. Weitz, and J. C. Baret, Langmuir **31,** 1127 (2015).

[7] B. Scheid, S. Dorbolo, L. R. Arriaga, and E. Rio, Phys. Rev. Lett. **109,** 264502 (2012).

[8] S. Dorbolo, H. Caps, and N. Vandewalle, New J. Phys. **5,** 161 (2003).

[9] See Supplemental Material at http://link.aps.org/supplemental/10.1103/PhysRevLett.120.054503 for stable production of uniform capsules.

[10] L. Hu, Y. Shen, W. Chen, and X. Fu, Int. J. Multiphase Flow **83,** 39 (2016).

[11] Y. Shen, L. Hu, W. Chen, and X. Fu, Phys. Fluids **29,** 047104 (2017).

[12] H. Aryafar and H. P. Kavehpour, Phys. Fluids **18,** 072105 (2006).

[13] H. Dong, W. W. Carr, and J. F. Morris, Phys. Fluids **18,** 072102 (2006).

[14] F. Blanchette and T. P. Bigioni, Nat. Phys. **2,** 254 (2006).

[15] A. A. Castrejón-Pita, J. R. Castrejon-Pita, and I. M. Hutchings, Phys. Rev. Lett. **108,** 074506 (2012).

[16] R. M. S. M. Schulkes, J. Fluid Mech. **309,** 277 (1996).

[17] J. Eggers, Phys. Rev. Lett. **71,** 3458 (1993).

[18] J. Eggers and E. Villermaux, Rep. Prog. Phys. **71,** 036601 (2008).

[19] J. R. Lister and H. A. Stone, Phys. Fluids **10,** 2758 (1998).

[20] R. Li, N. Ashgriz, S. Chandra, and J. R. Andrews, AIChE J. **54,** 3084 (2008).

[21] J. B. Keller, Phys. Fluids **26,** 3451 (1983).

[22] S. D. Hoath, S. Jung, and I. M. Hutchings, Phys. Fluids **25,** 021701 (2013).

[23] D. Lee and D. A. Weitz, Adv. Mater. **20,** 3498 (2008).

[24] R. T. Bartus, M. A. Tracy, D. F. Emerich, and S. E. Zale, Science **281,** 1161 (1998).

[25] K. A. Smith, J. M. Ottino, and M. Olvera de la Cruz, Phys. Rev. Lett. **93,** 204501 (2004).

[26] Y. Chen, X. Liu, and M. Shi, Appl. Phys. Lett. **102,** 051609 (2013).

[27] J. E. Silpe and D. W. McGrail, J. Appl. Phys. **113,** 17B304 (2013).

[28] J. Zou, C. Ji, B. G. Yuan, X. D. Ruan, and X. Fu, Phys. Rev. E **87,** 061002(R) (2013).

[29] P. G. Kim and J. Vogel, Colloids Surf. A **289,** 237 (2006).